Investigation of Negative Differential Resistance Phenomena in GaSb/AlSb/InAs/GaSb/AlSb/InAs Structures

Yeong-Her Wang, *Member, IEEE*, Meng Hwang Liu, Mau Phon Houng, J. F. Chen, and Alfred Y. Cho, *Fellow, IEEE*

***Abstract*—The negative differential resistance (NDR) phenomena were observed in GaSb/AlSb/InAs/-GaSb/AlSb/InAs resonant interband tunnel structures. Electron has resonantly achieved interband tunneling through the InAs/GaSb broken-gap quantum well. The InAs well width causes significant variations of the peak current density and NDR behaviors. The peak current density varies exponentially with the AlSb barrier thickness. The multiple NDR behavior was observed with appropriate InAs well and AlSb barrier thicknesses, e.g., 30 Å thick AlSb barrier and 240 Å wide InAs well. Only single negative resistance has, otherwise, been seen. The three-band model was used to interpret the effect of the InAs well and AlSb barrier on the current-voltage characteristics of GaSb/AlSb/InAs/GaSb/AlSb/InAs structures.**

I. Introduction

SINCE the proposal of the idea of resonant interband tunnel (RIT) by Sweeny *et al.* [1], much attention has been focused on devices incorporating interband as well as resonant tunneling in GaSb, InAs, and AlSb type II material systems [2], [3]. These devices have displayed new physical phenomena, such as electron-light-hole coupling induced tunneling. They also offer an alternative to quantum well (QW) or superlattice type I structures [4], [5] in obtaining high peak-to-valley current ratio (PVR) negative differential resistance (NDR) devices at room temperature [6]. Recently, GaSb/AlSb/GaSb/AlSb/InAs RIT structures with high PVR's operated at room temperature have been demonstrated [7], [8]. The valley current has been calculated and mainly attributed to the hole tunneling current [9], and therefore, the PVR can be improved by incorporating an InAs blocking layer into the AlSb/GaSb/AlSb region, i.e., GaSb/AlSb/InAs/GaSb/AlSb/InAs broken-gap structure [10], to reduce the hole tunneling current. The proposed structure has been realized and found to have PVR four to five times higher than that of the double-barrier RIT structures [10]. In addition to the high PVR (up to 20) when incorporating InAs, the peak current density is a figure of merit in NDR characteristics. A significant variation of the peak current density with InAs well width was found and the multiple NDR behaviors were also observed which were absent in the double-barrier RIT structure [10]. On the other hand, AlSb barrier thickness also has pronounced influence on the peak current density and the multiple NDR behavior.

As the evidence shown, a detailed analysis both theoretically and experimentally is worthy to be given in order to understand the physical insights of carrier transport in the broken-gap well. Based on this structure, the AlSb/InAs/GaSb/AlSb forms the broken-gap well where electrons and light holes could form coupled subbands. Multiband method [11] must be taken into account of this effect in E-k relation and boundary conditions. Previously, a two-band model proposed by Söderström *et al.* [12], which considered the coupling between the conduction band and light-hole band, was used to investigate the characteristics of the interband tunnel devices. However, a three-band model [13] incorporating the coupling effect of the spin split-off band has been proven to achieve better agreement with the experiments and is used here to investigate the characteristics of this kind of the structure. The peak current density predicted with the three-band model is in agreement with the experiments for GaSb/AlSb/InAs single-barrier interband tunnel structures and GaSb/AlSb/GaSb/AlSb/InAs RIT structures [13], in which electron-light-hole coupling induced tunneling is clearly dominant in main peak current. However, in the structures with GaSb/InAs interfaces, i.e., broken-gap structure, or with GaSb as the emitter, the carrier transport in tunneling may not be totally light-hole tunneling dominant. The heavy hole states also play an important role affecting I-V characteristics. Though the effect of the heavy hole states is unavoidable, the light-hole tunneling appears to be a major part of the main peak current due to the stronger light particle coupling. This point of view will briefly discussed in Section II.

The effects of the InAs well on the current-voltage (I-V) characteristics of the proposed structures, especially on the peak current density, are investigated in Section IV-B. The effect of AlSb barrier is discussed in Section IV-C. Calculations made here could interpret the observation of multiple NDR behavior due to the electron-light-hole coupling.

II. Theory

Fig. 1(a) shows the band diagram together with the material parameters employed here for GaSb/AlSb/GaSb/AlSb /InAs double barrier RIT structure [8]. The band diagram,

Manuscript received November 26, 1993; revised June 6, 1994. The review of this paper was arranged by Associate Editor S. Furukawa. This work was supported in part by the National Science Council of the Republic of China under contracts NSC-83-0417-E006-004.

Y.-H. Wang, M. H. Liu, and M. P. Houng are with the Department of Electrical Engineering, National Cheng-Kung University, Tainan, Taiwan, ROC.

J. F. Chen is with the Department of Electrophysics, National Chiao-Tung University, Hsinchu, Taiwan, ROC.

A. Y. Cho is with AT&T Bell Laboratories, Murray Hill, NJ 07974 USA.

IEEE Log Number 9404172.

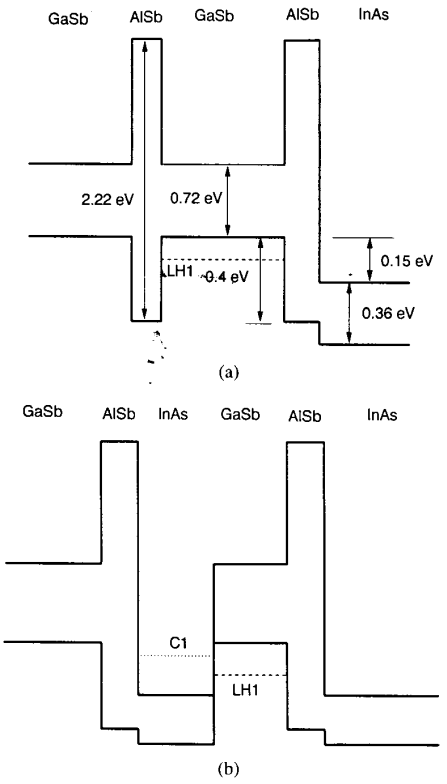

Fig. 1. The band diagrams of the (a) GaSb/AlSb/GaSb/AlSb/InAs and (b) GaSb/AlSb/InAs/GaSb/AlSb/InAs resonant interband tunneling structure.

incorporating an InAs as the blocking layer, of the proposed GaSb/AlSb/InAs/GaSb/AlSb/InAs broken-gap RIT structure is shown in Fig. 1(b).

In the envelope function approximation [14], [15], the wavefunction can be written as

$$\psi(r,t) = \sum_j u_{j0}(r) F_j(r,t) \tag{1}$$

where F_j satisfies

$$\sum_{j'} H_{jj'} F_{j'} = E F_j \tag{2}$$

are slowly varying envelope functions and u_{j0} are the periodic parts of the Bloch functions at $k = 0$. We take the z-axis to be the growth direction, the electronic motion inside each layer is described by k_z and $\vec{k_{\|}} = (k_x, k_y)$ of each layer. In the Γ-point transport we assume $\vec{k_{\|}} = 0$, the heavy-hole band decouples and the transport around Γ point is discussed. In the p-type GaAs/AlAs structures, the overall current as well as the relative magnitudes of the current peaks are strongly affected by the heavy and light hole band mixing [16]. In that kind of structure, the incoming holes are almost in the heavy hole states due to the larger density of states. However, in the InAs/AlSb/GaSb-based interband tunnel structures we studied, the incoming carrier is the light particle (electron) and its coupling with the light particle (light hole) is stronger than that with the heavy particle (heavy hole). As a consequence, as far as the transport mechanism of the main peak current is concerned, the contribution of the electron-light-hole coupling induced tunneling is more important than that of the heavy-hole tunneling. This particular phenomenon results from the unique band lineup in the InAs/AlSb/GaSb material system. In this paper, the contribution of the electron-light-hole coupling induced tunneling to the main peak current density is mainly concerned. However, for nonzero $\vec{k_{\|}}$ the heavy-hole band do affect the carrier transport of RIT structures, especially for the structures with the GaSb/InAs interfaces in which the coupling between electron and heavy-hole may not be neglected due to the absence of AlSb barrier. In addition, the band-mixing between light-hole and heavy-hole band is significant with large $k_{\|}$ [17]. The electron-heavy-hole coupling and heavy hole-light hole mixing will introduce the additional effects in the carrier transport. It may reduce or enhance the light-hole tunneling current and yields kinks or small peaks in the room-temperature or low-temperature I-V characteristics. The effect of the heavy hole states needs further consideration and is now under investigation.

Based on the framework of Luttinger and Kohn [11], the three-band Hamiltonian can be obtained as follows:

$$\begin{bmatrix} E_c - E & -\sqrt{\frac{2}{3}}\Pi\hbar k_z & \frac{1}{\sqrt{3}}\Pi\hbar k_z \\ -\sqrt{\frac{2}{3}}\Pi\hbar k_z & E_v - E & 0 \\ \frac{1}{\sqrt{3}}\Pi\hbar k_z & 0 & E_s - E \end{bmatrix} \begin{bmatrix} F_c \\ F_l \\ F_{\mathrm{so}} \end{bmatrix} = 0 \tag{3}$$

where F_c, F_l, and F_{so} are the envelope functions of the conduction band, light-hole band, and spin split-off hole band; E_c, E_v, and E_s are the band edges of the conduction band, light-hole band, and split-off hole band; $\hbar$ is the Planck's constant and

$$\Pi = \frac{1}{m_0}\langle S|P_z|Z\rangle \tag{4}$$

reflects the strength of coupling between the conduction band and valence band. The value of Π is extracted from the related data from Chang [18].

The E-k relation can be directly obtained from the three-band Hamiltonian

$$k_z = \sqrt{\frac{(E - E_c)(E - E_v)(E - E_v - \Delta)}{\left(E - E_v + \frac{2}{3}\Delta\right)\left(\Pi^2\hbar^2\right)}} \tag{5}$$

where Δ is the splitting energy $(E_v - E_s)$.

From the continuity condition, we can obtain the boundary conditions as follows:

$$F_c \tag{6}$$

$$\Pi^2\left(\frac{2}{E - E_v} + \frac{1}{E - E_s}\right)\frac{dF_c}{dz} \tag{7}$$

are continuous at the interfaces.

We can utilize the E-k relation and boundary conditions described above to find the transmission coefficients with the aid of the transfer matrix or scattering matrix method [19] both are stable in the calculation. Finally, the tunneling current density from the electron-light-hole coupling can be calculated

by the expression

$$J(V_A) = (2em^*/(2\pi)^2\hbar^3)\int_0^\infty dE_l \times \int_0^\infty dE_t T_c(E, E_t)[f_N(E) - f_1(E + eV_A)] \quad (8)$$

where $f_1(E)$ and $f_N(E)$ are the Fermi-Dirac distribution functions in layers 1 and N. V_A is the applied voltage across the active region, m^* is the effective mass, k is the Boltzmann constant, T is the absolute temperature, T_c is the transmission coefficient.

The detailed derivation of the E-k relation and boundary conditions suitable for the three-band model can be seen elsewhere [13].

In the calculation, the potential profiles in the structures are obtained by solving Poisson's equation, the parasitic and series resistance are not considered, the voltage across the cap layers and undoped InAs and GaSb spacer layers are also not considered.

III. Experimental

The proposed GaSb/AlSb/InAs/GaSb/AlSb/InAs structures were grown by molecular beam epitaxy [20] in a Riber 2300 system. Starting from the Zn-doped p-type GaAs substrate, followed by a 0.5 μm to 1 μm thick Be-doped p^+-GaSb buffer layer with a doping concentration of 5×10^{18} cm^{-3}, 100 Å thick undoped GaSb spacer, undoped AlSb barrier (15 or 30 or 45 Å), undoped InAs blocking layer, undoped GaSb layer of 65 Å, undoped AlSb barrier, 100 Å thick undoped InAs spacer and finally a 0.5 μm thick n$^+$−InAs cap layer, doped with a concentration of 1×10^{18} cm^{-3} using SnTe as the dopant [21], was deposited. The detailed growth conditions were previously reported in [22]. GaSb films of high quality grown on GaAs substrate could be obtained, despite a 7.2% lattice mismatch existing between GaSb epilayer and GaAs substrate. The stress has already been released in this GaSb thickness range on GaAs substrate and has been checked by the photoreflectance measurement[1]. The undoped InAs layers were grown in the In-stabilization conditions and show lightly n-type. The width of the blocking InAs well were in the range up to 300 Å. The undoped AlSb layers have relatively high resistivity. The diodes with a 50 μm diameter were fabricated by Au/Ge contact metallization, followed by a wet chemical mesa-isolation etching using the metal as an etching mask.

IV. Results and Discussion

A. Experimental Results for 30 Å Thick AlSb Layer

The room temperature I-V characteristics for InAs:30, 60, 120, 240, and 300 Å with GaSb:65 Å and AlSb:30 Å are illustrated in Fig. 2, where the GaSb electrode is applied positively with respect to the InAs electrode under forward bias.

[1] Unpublished data.

The I-V characteristics with a high PVR of 20 and a peak current density of 1.92 KA/cm^2 for 30 Å wide InAs well at room temperature are depicted in Fig. 2(a). The InAs well acts as a blockade of tunneling holes so that valley currents of GaSb/AlSb/InAs/GaSb/AlSb/InAs structures are suppressed, the PVR therefore increases as expected, compared with 5 of double-barrier RIT structure [8]. The peak current density decreases to 0.82 KA/cm^2 with a PVR of 12 for 60 Å wide InAs well. The peak current density for 300 Å wide InAs well is 0.92 KA/cm^2, with a PVR of 1.8. For 30, 60, and 300 Å wide InAs wells, only one distinct peak is seen in I-V characteristics at room temperature. While for 120 Å wide InAs well, two other small kinks are also observed. However, for 240 Å wide InAs well, two clear NDR regions are depicted. The peak current densities in two peaks are 0.86 KA/cm^2 and 1.02 KA/cm^2 with PVR's of 2.5 and 1.7, respectively.

B. Effects of InAs Blocking Layer in GaSb/AlSb/InAs/GaSb /AlSb/InAs Structures

The calculated peak current density and normalized peak current density of the proposed structures as a function of the InAs well width with AlSb barrier and GaSb well fixed at 30 Å and 65 Å are shown in Fig. 3. The experimental data are also marked in the figure. The normalized peak current density is relative to the zero-width InAs well, i.e., GaSb/AlSb/GaSb/AlSb/InAs structure. Reasonable agreements between the experimental and calculated peak current density are observed. Because only electron-light-hole coupling is explicitly included in the calculation, it reveals that the contribution of electron-light-hole coupling to the main peak current density of the proposed structures is important. The experimental peak current density is larger than that derived from calculation is partly due to the smaller AlSb barrier layer thickness than expected, from the estimation of transmission electron microscope (TEM). It was found experimentally that the peak current density first increases slightly with small InAs well width until to about 30 Å, then decreases with the InAs well width. Using the three-band model, the peak current density first increases from 0 to 10 Å wide InAs well, then decreases with increasing InAs well width until to 75 Å wide InAs well. The calculated transmission coefficients as a function of energy for InAs well width of 0, 5, 15, and 30 Å are shown in Fig. 4, where the energy is measured upward from the InAs conduction-band edge. In GaSb/AlSb/GaSb/AlSb/InAs (Fig. 1(a)), there is only a GaSb ground light-hole subband (LH1) in the energy overlap region between InAs conduction band and GaSb valence band. When intervening a small InAs layer, the incorporated InAs layer and GaSb well form broken-gap structure and the imperfect matching of the InAs conduction-band and GaSb valence-band wave functions leads to an effective potential barrier at the GaSb/InAs interface [23]. The barrier height (band discontinuity) of the GaSb/InAs interface (0.51 eV) is larger than that of the original GaSb/AlSb interface (0.4 eV), leading to better well confinement. In addition, the wider the InAs well is, the broken-gap structure provides the better confinement to GaSb. The stronger well confinement leads to the sharper

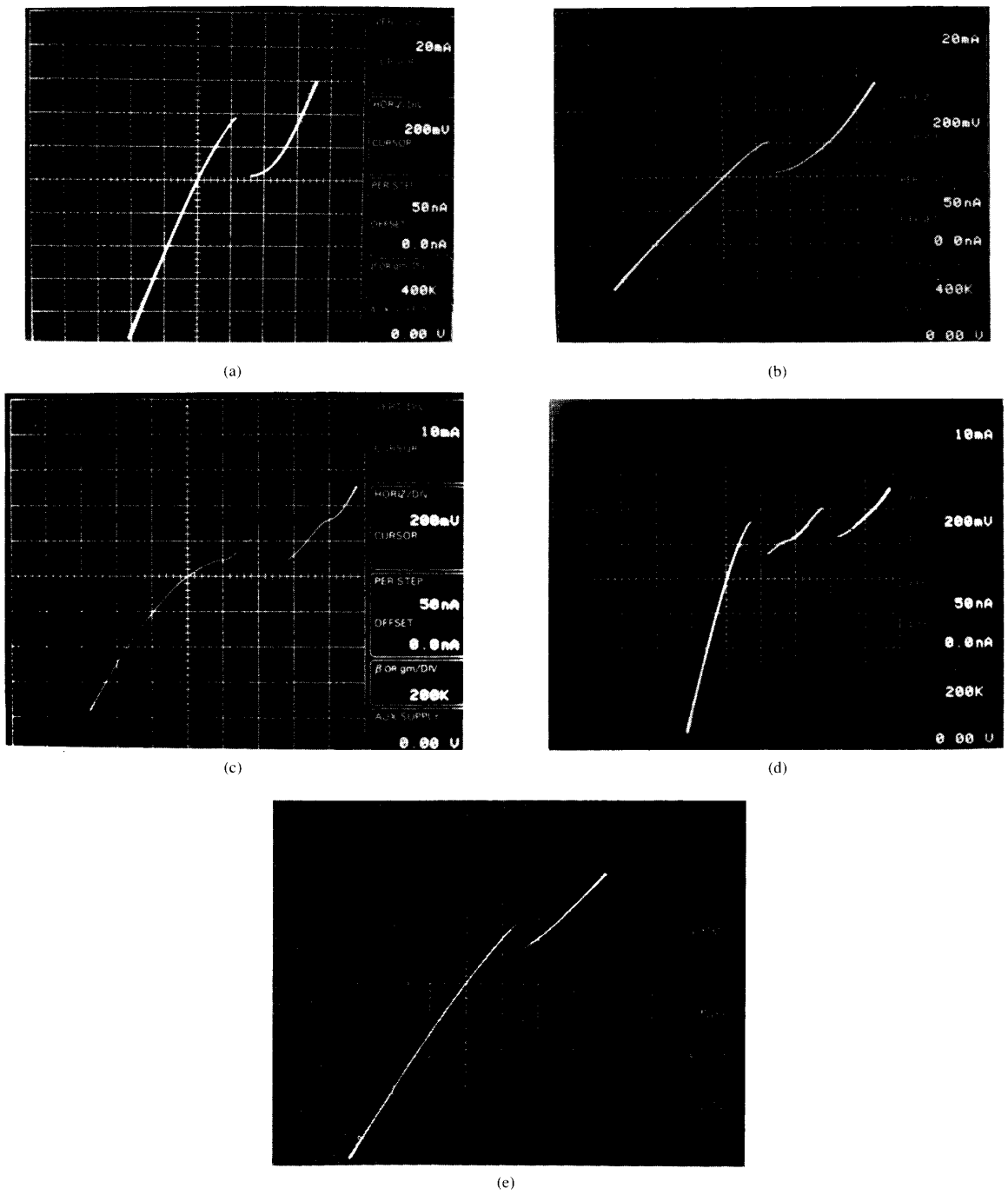

Fig. 2. The 300 K I-V characteristics of GaSb/AlSb/InAs/GaSb /AlSb/InAs structure with GaSb:65 Å, AlSb:30 Å and InAs: (a) 30 Å, (b) 60 Å, (c) 120 Å, (d) 240 Å, and (e) 300 Å, I = 10 mA/div, V = 200 mV/div.

transmission coefficient and the approach of LH1 in GaSb well to the InAs conduction-band edge. That makes more electrons to tunnel through LH1 due to the Fermi-Dirac distribution. On the other hand, there is no conduction subband in InAs well appearing in the energy overlap region with a small InAs well, the transmittivity through the well region decreases so that less electrons can tunnel through this region. These two competing mechanisms are responsible for the transport mechanism in peak current of the proposed structure from 0 to 90 Å wide InAs well. With a small InAs well, the former dominates and

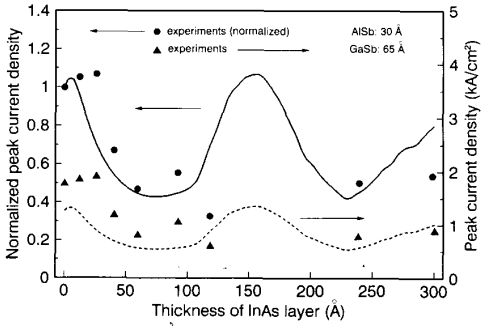

Fig. 3. The calculated peak current density of the proposed structure as a function of the InAs well width with AlSb barrier and GaSb well fixed at 30 Å and 65 Å. The experimental data are also marked. The normalized peak current density is relative to the zero-width InAs well.

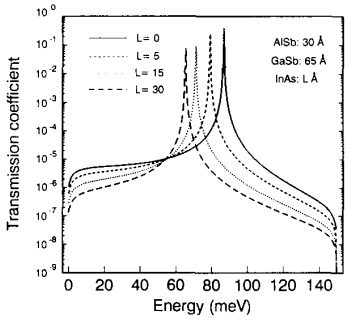

Fig. 4. The transmission coefficients as a function of energy with InAs well width of 0, 5, 15, and 30 Å. All the structures have 65 Å and 30 Å wide GaSb and AlSb.

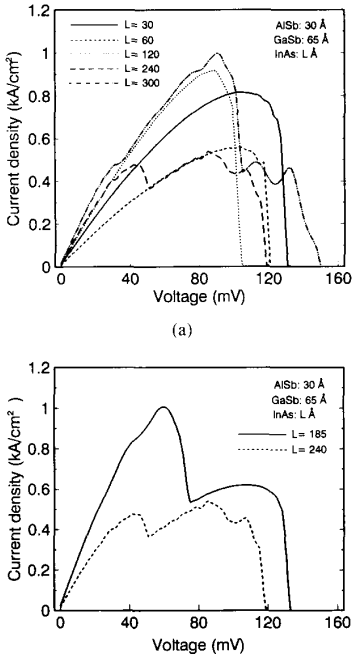

Fig. 5. (a) The calculated tunnel current versus voltage curves for InAs well width of 30, 60, 120, 240, and 300 Å with GaSb:65 Å and AlSb:30 Å, for comparison with the experiments (Fig. 2). (b) The calculated tunnel current versus voltage curves for 185 and 240 Åwide InAs well.

the peak current density is increased. With increasing InAs well width, the latter dominates and hence the peak current density is decreased. However, a deviation exists in comparing the experiment with the calculated result for 30 Å wide InAs well. The normalized experimental peak current density is larger than 1, while the calculated result is otherwise. This may be either attributed to the pinning of LH1, not decreased in energy as in the calculated transmission coefficient, resulting from the interface states at the GaSb/InAs interface so that the peak current density maintains nearly constant, or to the effect of the heavy hole states. This point of view need further verification.

When the InAs well width is larger than 90 Å, the ground conduction subband (C1) in InAs well appears in the energy overlap region and contributes to the current density. As the InAs well width is increased, LH1 in GaSb well and C1 in InAs well shift to the InAs conduction-band edge, the peak current density gradually increases due to the tunneling of more electrons in InAs emitter through LH1, and C1 also contributes to the current density. For direct comparison with the experiments, the calculated tunnel current versus applied voltage curves for InAs: 30, 60, 120, 240, and 300 Å are shown in Fig. 5(a). As in Figs. 2(a), (b), and 5(a) (for 30 and 60 Å wide InAs wells), only one distinct NDR peak is observed in the calculated results as in the experiments. However, deviations exist in the case of 120 Å wide InAs well. The normalized calculated peak current density is higher than that in experiment, in contrast to other cases. In addition, two kinks as well as one distinct NDR peak are observed in the experimental I-V characteristics which are not expected in the calculated result (Fig. 5(a)). The lowering of the peak current density and observation of kinks may be attributed to the effect of the heavy hole states with large $\vec{k}_{\|}$. With large $\vec{k}_{\|}$, the heavy hole-light hole mixing would reduce the contribution of pure light-hole tunneling [17] and hence the peak current density. The two kinks may also result from the tunneling of heavy-hole subbands (possibly through HH2 and HH1). Of course, there can be some possible transport mechanisms leading to the additional phenomena. When InAs well width is increased above 155 Å, the tunneling through LH1 is cut off, i.e., below the conduction-band edge of InAs emitter, at smaller voltage and then the peak current density is decreased. On the other hand, C1 contributes to the current density at a higher voltage and may form a "shoulder" in the I-V curve as shown in Fig. 5(b), where that with 185 Å wide InAs well is depicted as an example.

When the InAs well width is larger than 185 Å, the second conduction subband (C2) appears in the energy overlap region and C1 crosses LH1 after the subband-interaction-induced repulsion [24]. Simultaneously, C1 and LH1 still shift to the InAs conduction-band edge with the increasing InAs well width. From 190 to 220 Å wide InAs well, C1 and LH1 are close in energy and are dominant contributions to the peak current. However, with increasing InAs well width, the cutoff

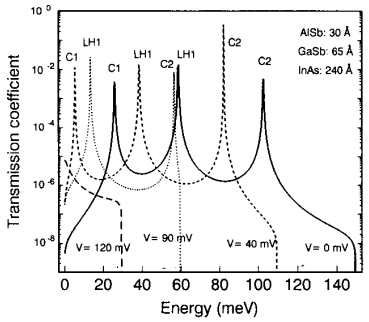

Fig. 6. The variation of the transmission coefficient with voltage across the active region for the 240 Å wide InAs well.

of tunneling through C1 and LH1 happens at smaller and smaller voltage so that the peak current is decreased. On the other hand, C2 contributes to the current density and forms a shoulder in I-V curve. Since C2 shifts to the InAs conduction-band edge with InAs well width, the Fermi-Dirac distribution in InAs emitter allows more electrons to tunnel through it and the current density in the shoulder may rise to form another peak in I-V curve at higher voltage. C2 in InAs well is the dominant contribution to the second peak in I-V characteristics and this is the reason why GaSb/AlSb/InAs/GaSb/AlSb/InAs structures with a 240 Å wide InAs well has the multiple NDR behavior in I-V characteristics. In Fig. 5(b), the calculated tunneling current density versus voltage curve with a 240 Å wide InAs well is also shown. We can see that there is one peak in I-V curve at voltage around 45 mV with a PVR of 1.5 and another peak at voltage around 90 mV. The variation of the transmission coefficient with the applied voltage for 240 Å wide InAs well is shown in Fig. 6. At 40 mV, C1 and LH1 approach to the InAs conduction-band edge and contribute to the first peak. With the voltage is further increased, the current density decreases due to the cutoff of tunneling through C1, then increases again due to the approach of LH1 and C2 to the InAs conduction-band edge, where a valley would be formed and the first NDR is thus observed. Similarly, LH1 and C2 contribute to the second peak and then would be cut off by the collector GaSb bandgap with increasing voltage, where the second NDR is formed. The multiple NDR behavior is owing to the contribution of the different subbands which are spaced enough in energy (Fig. 6). On the other hand, for InAs: 30, 60, 120 Å, only single NDR observed in I-V characteristics is attributed to that LH1 is the dominant contribution to the peak current density.

However, just only single NDR is observed in the experimental I-V characteristics for 300 Å wide InAs well (Fig. 2(e)). Fig. 7(a) shows the calculated current density versus voltage curves with InAs wide width of 255, 280, and 300 Å. In this range of InAs well width, only single NDR peak can be found as in the experiment. Though the number of the subbands increases, the spacing in energy between the subbands has been reduced. Fig. 7(b) shows the variation of the transmission coefficient with the applied voltage for a 300 Å wide InAs well. There are four subbands, C1, LH1, C2,

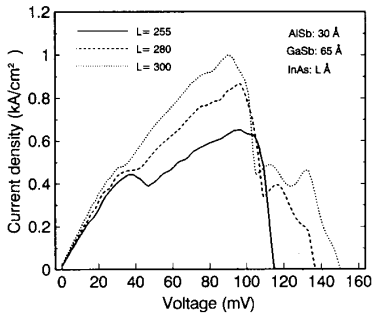

(a)

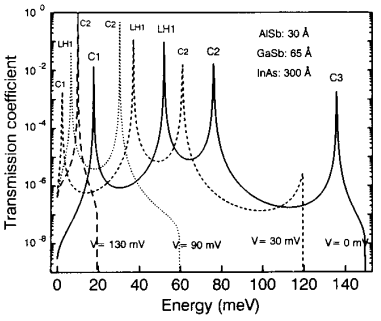

(b)

Fig. 7. (a) The calculated current density versus voltage curves with InAs well width of 255, 280, and 300 Å for GaSb: 65 Å and AlSb:30 Å. (b) The variation of the transmission coefficient with the voltage for a 300 Å wide InAs well.

and C3, in the energy overlap region. At low voltage (30 mV), C3 is cut off by the collector GaSb bandgap and has no contribution to the current density. In this time, C1 is the dominant contribution to the current density. When the voltage is increased, the tunneling through C1 is cut off and peak current density decreases slightly but rises soon again because LH1 approaches to the InAs conduction-band edge and contributes dominantly to the current density (from 30 to 90 mV). With further increase in voltage, the tunneling through LH1 is cut off and the current density decreases abruptly, the NDR is then formed. Finally, the tunneling through C2 contributes a few current densities at higher voltage (130 mV), which may be covered by the valley current components so that the contribution from C2 is not observed in the experimental I-V characteristics.

C. Effects of AlSb Barrier in the GaSb/AlSb/InAs/GaSb/AlSb/InAs Structures

As thickness of AlSb (both barriers) changes from 15 Å to 45 Å with 60 Å-wide-InAs and 65 Å-wide-GaSb, not much difference is expected except for the reduced FWHM (full-width-half-maximum) and transmitivity. In the experiments, the peak current density for 15 Å thick AlSb layer is larger than that of 30 Å thick AlSb barrier. However, the NDR characteristics is better in the structure with 30 Å thick AlSb barriers on account of PVR. The NDR characteristics in 45 Å

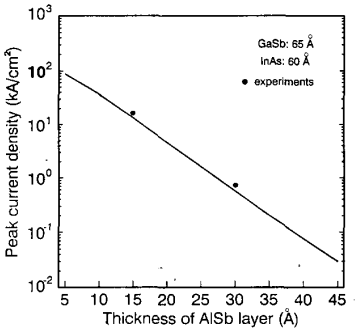

Fig. 8. The calculated peak current density as a function of AlSb layer thickness with GaSb:65 Å and InAs:60 Å.

thick AlSb are barely observed, only a shoulder, on account of the low transmitivity so that the tunneling current may be covered by other current paths, such as thermionic current. Fig. 8 shows the calculated peak current density as a function of AlSb layer thickness with 65 and 60 Å wide GaSb and InAs wells. The peak current density varies exponentially with the AlSb layer thickness. As the actual layer thickness of AlSb barrier is less than that expected, resulting in the larger peak current density than those calculated shown in Figs. 3 and 8. The trend of calculation is in agreement with that of the experiments. Fig. 9 shows the room temperature characteristics for InAs:240 Å with GaSb:65 Å and AlSb:15 Å. Compared with Fig. 2(d), note the multiple NDR behavior shown for AlSb: 30 Å instead of AlSb:15 Å with a 240 Å wide InAs well. It is attributed to the widening FWHM such that the abrupt decrease in current density at smaller voltage fades out for AlSb:15 Å. The calculated current density versus voltage curves for InAs:230 and 240 Å with 15 Å thick AlSb and 65 Å wide GaSb are shown in Fig. 10. Theoretically, there still is a small NDR peak at smaller voltage as in the case for AlSb of 30 Å. However, because of the thin AlSb barrier of 15 Å, the other elastic and inelastic tunneling mechanisms cause the first NDR fade out and even disappear. The AlSb layer thickness also plays an important role on the multiple NDR behavior.

V. Conclusion

The incorporation of InAs as the blocking layer in GaSb/AlSb/InAs/GaSb/AlSb/InAs structures has been demonstrated in order to reduce the hole tunneling current and enhance the PVR's. The transport mechanisms of GaSb/AlSb/InAs/GaSb/AlSb/InAs broken-gap RIT structure are investigated on the basis of three-band $\vec{k} \cdot \vec{p}$ model with the aid of transfer matrix method. The importance of the contribution of the electron-light-hole coupling to the main peak current is emphasized. InAs width is found to be the most important role for the observation of I-V characteristics, it causes significant variations of the peak current. The peak current density of the proposed structure varies exponentially with the AlSb layer thickness. Device parameters dependent on new multiple NDR behavior are also presented and attributed to the subbands, which are spaced enough in energy, in the broken-gap well. AlSb layer thickness also gives considerable effect on the observation of the multiple NDR behavior.

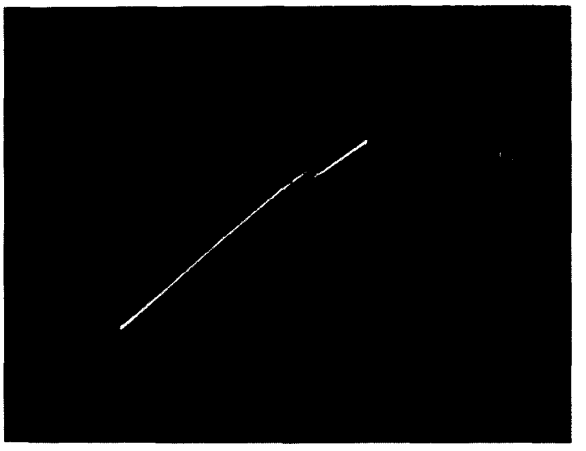

Fig. 9. The 300 K I-V characteristics of GaSb/AlSb/InAs/GaSb/ AlSb/InAs structure with GaSb:65 Å, AlSb:15 Å and InAs:240 Å.

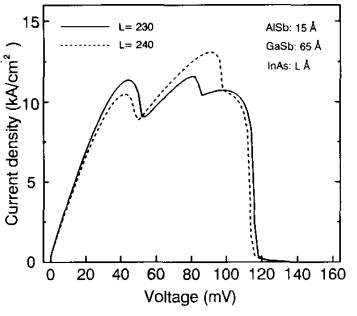

Fig. 10. The calculated current density versus voltage curves for InAs:230 and 240 Å with 15 Å thick AlSb and 65 Å wide GaSb.

Acknowledgment

Helpful discussions with C. L. Shen and H. H. Chen are highly appreciated.

References

[1] M. Sweeny and J. Xu, "Resonant interband tunnel diodes," *Appl. Phys. Lett.*, vol. 54, pp. 546–548, 1989.
[2] H. Takaoka, C. A. Chang, E. E. Mendez, L. L. Chang, and L. Esaki, "GaSb-AlSb-InAs multi-heterojunctions," *Physica*, vol. 117B, pp. 741–743, 1983.
[3] L. Yang, J. F. Chen, and A. Y. Cho, "New GaSb/AlSb/GaSb/AlSb/InAs/AlSb/InAs triple-barrier interband tunneling diode," *Electron. Lett.*, vol. 26, pp. 1277–1279, 1990.
[4] L. L. Chang, L. Esaki, and R. Tsu, "Resonant tunneling in semiconductor double barriers," *Appl. Phys. Lett.*, vol. 24, pp. 593–595, June 1974.
[5] S. Sen, F. Capasso, D. Sivco, and A. Y. Cho, "New resonant tunneling device with multiple negative resistance regions and high room temperature peak-to-valley ratios," *IEEE Electron Device Lett.*, vol. 9, pp. 402–404, 1988.
[6] J. R. Soderstrom, D. H. Chow, and T. C. McGill, "Demonstration of large peak-to-valley current ratios in InAs/AlGaSb/InAs single barrier structures," *Appl. Phys. Lett.*, vol. 55, pp. 1348–1350, 1989.
[7] L. Yang, J. F. Chen, and A. Y. Cho, "A new GaSb/AlSb /GaSb/AlSb/InAs double-barrier interband tunneling diode and its tunneling mechanism," *J. Appl. Phys.*, vol. 68, pp. 2997–3000, Sept. 1990.

[8] J. F. Chen, L. Yang, and A. Y. Cho, "Investigation of the influence of the barrier and the well thicknesses in GaSb/AlSb/GaSb/AlSb/InAs double-barrier interband tunneling structures," *IEEE Electron Device Lett.*, vol. 11, pp. 532–534, Nov. 1990.
[9] M. P. Houng, Y. H. Wang, and C. L. Shen, "The negative differential resistance characteristics of double-barrier interband tunneling structures," *J. Appl. Phys.*, vol. 70, pp. 4640–4642, Oct. 1991.
[10] M. P. Houng, Y. H. Wang, C. L. Shen, J. F. Chen, and A. Y. Cho, "Improvement of peak-to-valley ratio by the incorporation of the InAs layer into the GaSb/AlSb/GaSb/AlSb/InAs double barrier resonant interband tunneling structure," *Appl. Phys. Lett.*, vol. 60, pp. 713–715, Feb. 1992.
[11] J. M. Luttinger and W. Kohn, "Motion of electrons and holes in perturbed periodic fields," *Phys. Rev.*, vol. 97, pp. 869–883, 1955.
[12] J. R. Soderstrom, E. T. Yu, M. K. Jackson, Y. Rajakarunanyake, and T. C. McGill, "Two-band modeling of narrow band gap and interband tunneling devices," *J. Appl. Phys.*, vol. 68, pp. 1372–1375, 1990.
[13] M. H. Liu, Y. H. Wang, and M. P. Houng, "Carrier transport in InAs/AlSb/GaSb interband tunneling structures," *J. Appl. Phys.*, vol. 74, pp. 6222–6226, Nov. 1993.
[14] G. Bastard, "Superlattice band structure in the envelope function approximation," *Phys. Rev. B*, vol. 24, pp. 5693–5697, 1981.
[15] G. Bastard, "Theoretical investigation of superlattice band structure in the envelope function approximation," *Phys. Rev. B*, vol. 25, pp. 7584–7589, 1982.
[16] M. S. Kiledjian, J. N. Schulman, K. L. Wang, and K. V. Rousseau, "Hole and interband resonant tunneling in GaAs/GaAlAs and InAs/GaSb/AlSb tunnel structures," *Surface Science*, vol. 267, pp. 405–408, 1992.
[17] D. Z. Y. Ting, E. T. Yu, and T. C. McGill, "Role of heavy-hole states in interband tunneling structures," *Appl. Phys. Lett.*, vol. 58, pp. 292–294, 1991.
[18] Y. C. Chang, "Bond-orbital models for superlattices," *Phys. Rev. B*, vol. 37, pp. 8215–8222, 1988.
[19] D. Y. K. Ko and J. C. Inkson, "Matrix method for tunneling in heterostructures: resonant tunneling in multilayer systems," *Phys. Rev. B*, vol. 38, pp. 9945–9951, 1988.
[20] A. Y. Cho, "Growth of III-V semiconductor by molecular beam epitaxy and their properties," *Thin Solid Films*, vol. 100, pp. 291–317, 1983.
[21] J. F. Chen and A. Y. Cho, "Electrical characterizations of Te-doped GaSb grown by molecular beam epitaxy using SnTe," *J. Appl. Phys.*, vol. 68, p. 3040, 1991.
[22] J. F. Chen, M. C. Wu, L. Yang, and A. Y. Cho, "InAs/AlSb/GaSb single barrier interband tunneling diodes with high peak-to-valley current ratios at room temperature," *J. Appl. Phys.*, vol. 68, pp. 3040–3043, Sept. 1990.
[23] L. F. Luo, R. Beresford, K. F. Longenbach, and W. I. Wang, "Resonant interband coupling in single barrier heterostructures of InAs/GaSb/InAs and GaSb/InAs/GaSb," *J. Appl. Phys.*, vol. 68, pp. 2854–2857, 1990.
[24] M. H. Liu, Y. H. Wang, and M. P. Houng, "The effect of InAs thickness on the peak current density and subband properties of the GaSb/InAs/GaSb/AlSb/InAs structures," *J. Appl. Phys.*, vol. 75, pp. 2699–2705, 1994.

Yeong-Her Wang (M'88) was born in 1956. He received the B.S., M.S., and Ph.D. degrees in electrical engineering from the National Cheng Kung University, Taiwan, in 1978, 1980, and 1985, respectively. His doctoral research was in the area of molecular beam epitaxy and the applications to bulk barrier devices.

From 1982 to 1985, he was an Instructor and during 1985–1992 he was an Associate Professor of Electrical Engineering at the National Cheng Kung University, Taiwan. From 1989 to 1992 he engaged in postdoctoral research at AT&T Bell Laboratories, Murray Hill, NJ, where he worked on the MBE growth for the study of vertical-cavity surface-emitting lasers. He is currently a Professor at the National Cheng Kung University, where his research and teaching activities have focused on semiconductor device physics. His current interests are in the development and modeling of III-V compound semiconductor devices such as delta-doped GaAs resonant tunneling devices, interband resonant tunneling, negative differential resistance devices, heterostructure bipolar transistors, normal incident long-wavelength IR photodetectors, and vertical-cavity surface-emitting lasers.

Meng Hwang Liu was born in Taiwan, Republic of China, on November 28, 1968. He received the B.S. and M.S. degrees from the Department of Electrical Engineering, National Cheng Kung University, Taiwan, ROC, in 1990 and 1992, respectively. He is currently working toward the Ph.D. degree in electrical engineering at the National Cheng Kung University, where his research involves developing a simulation model for interband tunnel devices.

Mau Phon Houng was born in Taiwan, Republic of China, on June 20, 1952. He received the B.S. degree in physics from the National Cheng Kung University, the M.S. degree from the Institute of Material Engineering, National Tsing Hua University, and the Ph.D. degree in electrical engineering from the National Cheng Kung University, in 1978, 1980, and 1985, respectively. His current research interest is in the field of photoelectronic devices.

J. F. Chen received the B.S. and M.S. degrees in electronic engineering from the National Chiao Tung University in 1981 and the Ph.D. degree in electrical engineering from the State University of New York at Buffalo, NY, in 1989.

In 1989 he joined AT&T Bell Laboratories, Murray Hill, NJ, where he worked on MBE growth of compound semiconductors and related quantum tunneling effects. In 1991, he joined the Electrophysics Department at the National Chiao-Tung University, Taiwan. His research interests are MBE growth and fabrication of compound semiconductor devices.

Alfred Y. Cho (S'57–M'60–SM'79–F'81) received the B.S., M.S., and Ph.D. degrees in electrical engineering from the University of Illinois, Urbana, IL, in 1960, 1961, and 1968, respectively.

He joined AT&T Bell Laboratories, Murray Hill, NJ, in 1968, where he is presently Director of the Materials Processing Research Laboratory. His research accomplishments include the construction of a surface phase diagram for MBE crystal growth, the first fabrication of an MBE artificial superlattice, the first MBE IMPATT diode, mixer mode, a field effect transistor operating at microwave frequencies, and the first MBE double-heterostructure laser operating CW at room temperature. His recent work is in the area of quantum-well devices. He has published over 250 papers in surface physics, crystal growth, and semiconductor devices related to MBE.

Dr. Cho received the Electronics Division Award of the Electrochemical Society in 1977. He received the American Physical Society International Prize for New Materials and the IEEE Morris N. Liebmann Award in 1982, the University of Illinois Electrical and Computer Engineering Distinguished Alumnus Award, and the Chinese Institute of Engineers USA Distinguished Achievement Award in 1986, and the Solid State Science and Technology Medal of the Electrochemical Society in 1987. In 1988 he received the College of Engineering Alumni Honor Award of the University of Illinois, the World Materials Congress Award of ASM International, the Gaede–Langmuir Award of the American Vacuum Society, and the Industrial Research Achievement Award of the Industrial Research Institute, Inc. He is a Fellow of the American Physical Society as well as the American Academy of Arts and Sciences. He is a member of the American Vacuum Society, the Electrochemical Society, the Materials Research Society, the National Academy of Engineering, and the National Academy of Sciences.